# Nanoelectronics and Its New Materials – A NEW ERA OF NANOSCIENCE

**Nanoelectronics and Its New Materials –**
## A NEW ERA OF NANOSCIENCE

ZEISS
Seeing beyond

WILEY

**Discover the recent advances in electronics research and fundamental nanoscience.**

Nanotechnology has become the driving force behind breakthroughs in engineering, materials science, physics, chemistry, and biological sciences. In this compendium, we delve into a wide range of novel applications that highlight recent advances in electronics research and fundamental nanoscience. From surface analysis and defect detection to tailored optical functionality and transparent nanowire electrodes, this eBook covers key topics that will revolutionize the future of electronics.

To get your hands on this valuable resource and unleash the power of nanotechnology, simply download the eBook now. Stay ahead of the curve and embrace the future of electronics with nanoscience as your guide.

ZEISS

Seeing beyond

WILEY

# Dynamic Networks of Cellulose Nanofibrils Enable Highly Conductive and Strong Polymer Gel Electrolytes for Lithium-Ion Batteries

*Zhen Wang,\* Patrick Heasman, Jowan Rostami, Tobias Benselfelt, Mathieu Linares, Hailong Li, Artem Iakunkov, Farhiya Sellman, Rebecca Östmans, Mahiar Max Hamedi, Igor Zozoulenko, and Lars Wågberg\**

**Tunable dynamic networks of cellulose nanofibrils (CNFs) are utilized to prepare high-performance polymer gel electrolytes. By swelling an anisotropically dewatered, but never dried, CNF gel in acidic salt solutions, a highly sparse network is constructed with a fraction of CNFs as low as 0.9%, taking advantage of the very high aspect ratio and the ultra-thin thickness of the CNFs (micrometers long and 2–4 nm thick). These CNF networks expose high interfacial areas and can accommodate massive amounts of the ionic conductive liquid polyethylene glycol-based electrolyte into strong homogeneous gel electrolytes. In addition to the reinforced mechanical properties, the presence of the CNFs simultaneously enhances the ionic conductivity due to their excellent strong water-binding capacity according to computational simulations. This strategy renders the electrolyte a room-temperature ionic conductivity of 0.61 ± 0.12 mS cm$^{-1}$ which is one of the highest among polymer gel electrolytes. The electrolyte shows superior performances as a separator for lithium iron phosphate half-cells in high specific capacity (161 mAh g$^{-1}$ at 0.1C), excellent rate capability (5C), and cycling stability (94% capacity retention after 300 cycles at 1C) at 60 °C, as well as stable room temperature cycling performance and considerably improved safety compared with commercial liquid electrolyte systems.**

## 1. Introduction

Lithium-ion batteries (LIBs) power a wide range of electronic devices and vehicles.[1,2] The unremitting pursuit for high-performance batteries urges the development of novel electrolytes with high ionic conductivity, good electrochemical stability, strong mechanical properties, and safety.[3] Compared to conventional liquid electrolytes with flammable organic solvents, solid-state electrolytes are safer and compatible with Li metal anodes, which makes them ideal candidates for next-generation LIBs.[4] Polymer gel electrolytes have an advantage in processability and light-weight while their flexibility enables conformal interface with battery electrodes that is difficult to achieve with inorganic (ceramic) electrolytes.[5–7] The limitation of polymer electrolytes for practical applications, however, is the relatively low ionic conductivity, especially at lower temperatures.

Polyethylene oxide (PEO), also referred to as polyethylene glycol (PEG), is the most widely used polymer for battery electrolytes.[8,9] PEO dissolves lithium salts by complexing its oxygen atoms with lithium-ions (Li-ion). The complexed Li-ion is suggested to hop along the polymer segments to conduct charges when an electrical field is applied.[10] To suppress crystallinity and thus improve the ionic conductivity of PEO-based electrolytes,

Z. Wang, J. Rostami, T. Benselfelt, A. Iakunkov, F. Sellman, R. Östmans,
M. M. Hamedi, L. Wågberg
Division of Fibre Technology
Department of Fibre and Polymer Technology
KTH Royal Institute of Technology
Teknikringen 56, 10044 Stockholm, Sweden
E-mail: zhenwang@kth.se; wagberg@kth.se

F. Sellman, R. Östmans, L. Wågberg
Wallenberg Wood Science Centre
Department of Fibre and Polymer Technology
KTH Royal Institute of Technology
Teknikringen 56, 10044 Stockholm, Sweden

P. Heasman, M. Linares, I. Zozoulenko
Laboratory of Organic Electronics
Department of Science and Technology
Linköping University
60174 Norrköping, Sweden

I. Zozoulenko
Wallenberg Wood Science Center
Linköping University
60174 Norrköping, Sweden

H. Li
Department of Physics
AlbaNova University Center
Stockholm University
10691 Stockholm, Sweden

two approaches are widely adopted. One is the incorporation of plasticizers,[11,12] which are normally low-molecular-weight species that enhance the segment mobility of the polymer. This approach, however, generally couples the enhanced ionic conductivity with unfavorable mechanical properties, i.e., the higher conductivity the more liquid-like state.[11,13] The other approach is blending nanoscale fillers into the polymer electrolytes which makes them mechanically robust. The large area of the interface created between the electrolyte and the filler is believed to provide a continuous highway for Li-ion hopping, especially for nanofillers in the form of 1D nanowires.[4,14,15] In such an approach, the load of nonconductive filler has to be as low as possible to minimize the inactive volume that compromises the ionic conductivity.[16]

Cellulose nanofibrils (CNFs) are an ideal candidate as the filler for PEO-based electrolytes for at least four reasons:[17] i) derived from wood, they are abundantly available and have one of the lowest prices ($2-35 per gram of dry CNFs[18]) amongst the bulk products of low-permittivity nanomaterials; ii) CNFs have the finest feature size (2-4 nm thick)[19] which is especially favored for nanocomposites due to the possible ultrahigh surface area (estimated to be 670 m$^2$ g$^{-1}$, see the experimental section for details); iii) CNFs' very high aspect ratio (micrometers long versus 2–4 nm thick) and high modulus estimated to 88–110 GPa[20] promises mechanically strong networks at very low concentrations (as low as 0.5 wt% in water);[21] iv) the abundant functional groups[22] of CNFs may create a favorable interaction with the electrolyte components to enhance the dissolution of Li salts[23] and to reinforce mechanical properties of PEO-based composites.[24]

Efforts have been made to form nanocellulose/PEO composites for battery electrolytes,[16,24–27] where the potential of nanocellulose was not fully explored due to the aggregation or the lack of control in the orientation of the cellulose nanomaterials. In this study, we present a novel strategy to utilize CNF networks with tailored pore structure to accommodate a PEG-based electrolyte for high-performance LIBs. By swelling CNF gels in acidic salt solutions, dynamic networks of CNFs were obtained with a tunable pore structure where the ultra-thin thickness of the CNFs, 2–4 nm, was well preserved. The high aspect ratio of the CNFs allows an ultra-low fraction of CNFs hosting a large amount of the liquid PEG-based electrolyte into a seemingly solid homogeneous gel. Such a strategy decouples the detrimental relationship between mechanical properties and molecular mobility (conductivity), allowing for high conductivity close to that of liquid electrolytes and high mechanical performance created by the gel material. The application of the CNF/PEG electrolytes in high-performance and safe LIB is also demonstrated.

## 2. Results and discussion

### 2.1. Tunable Properties of CNF/PEG Electrolytes

Previously, we reported the discovery of dynamic CNF networks.[28] In this work, we for the first time incorporate the liquid PEG-based electrolyte into the dynamic CNF networks to achieve polymer gel electrolytes with tunable properties. As schematically shown in **Figure 1**a, first, we prepared the wet filter cake of CNFs by filtrating the aqueous dispersion of carboxylmethylated CNFs. The nanofibrils formed a loose network with an orientation in the *x-y* plane where the joints were moderately physically cross-linked[29] and the micropores were filled with water. The wet CNF membranes were then first soaked in NaCl solutions of different concentrations, by which we achieved the dynamically anisotropic swelling perpendicular to the *x-y* plane (i.e., in the *z*-axis direction) while maintaining a constant diameter. The swollen gels were then protonated at pH 2, which improved their strength and the electrochemical and cycling stability of the final CNF/PEG electrolyte due to a lower degree of hydration.[30] Further, by using a controlled, gradual solvent exchange from water to ethanol and then to acetone (see experimental section for details) followed by an infusing of the liquid-state PEG electrolyte consisting of PEG,
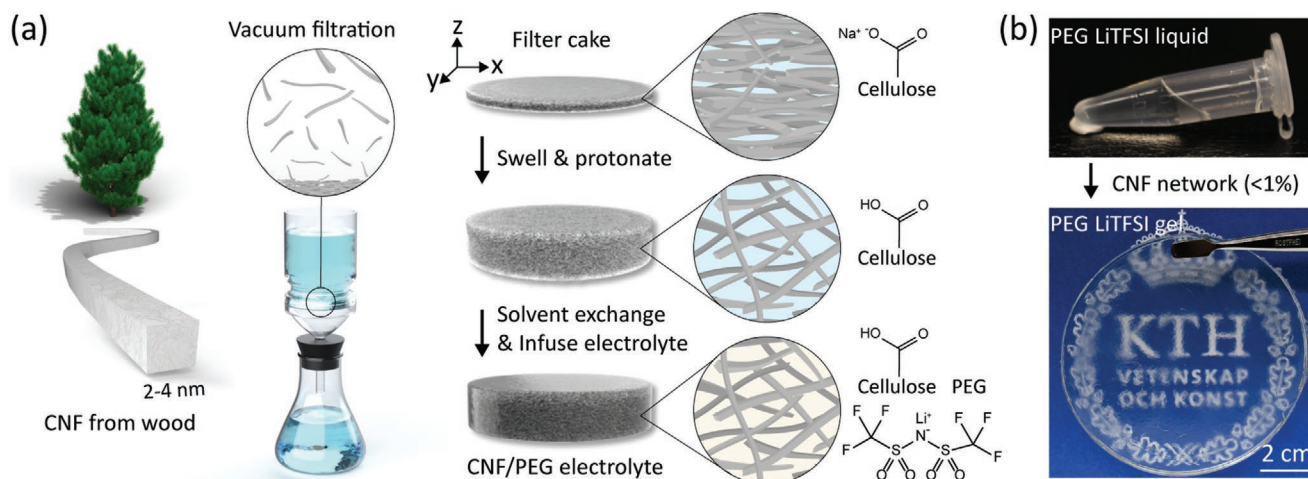


**Figure 1.** Preparation of the CNF/PEG electrolyte. a) Schematic illustration of the preparation procedure; b) a photo of the PEG/LiTFSI electrolyte and the electrolyte infused membrane.
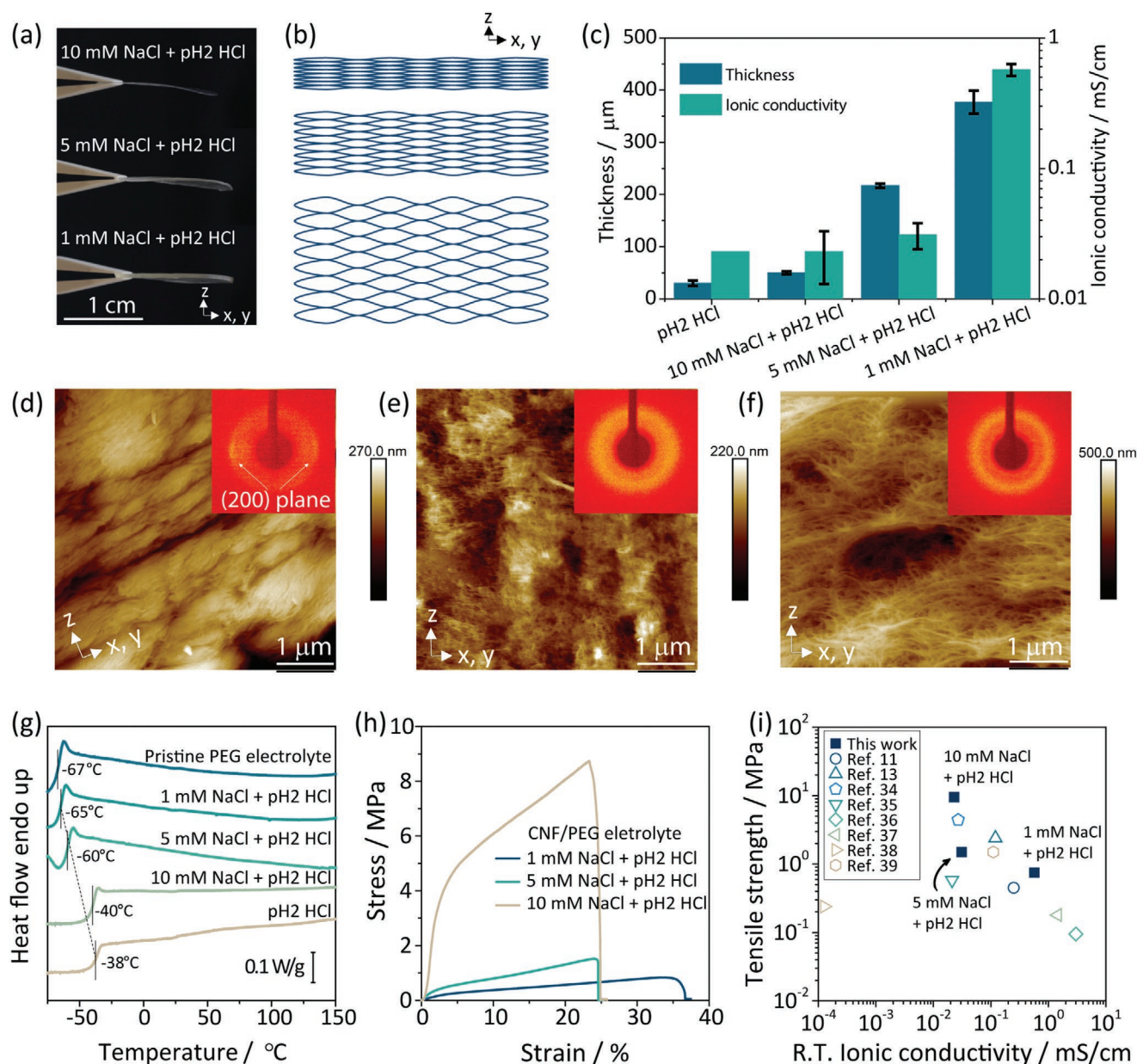
**Figure 2.** CNF/PEG electrolytes with tunable properties. a) Photos showing the thickness difference of the CNF/PEG electrolytes; b) schematic illustration of the pore structure difference induced by swelling in the NaCl solutions of various concentrations; c) thickness and ionic conductivity of the CNF/PEG electrolytes; cross-sectional AFM images and 2D WAXS patterns of the CNF/PEG electrolytes with CNFs pretreated by d) 10 mM NaCl + pH2 HCl, e) 5 mM NaCl + pH2 HCl, and f) 1 mM NaCl + pH2 HCl; g) DSC curves and h) tensile stress-strain curves of the CNF/PEG electrolytes; i) comparison of the ionic conductivity and the tensile strength of the CNF/PEG electrolytes with previous reports including all types of PEG(O)-based electrolytes (more details in Table S1, Supporting Information).

succinonitrile (SCN), and lithium bis(trifluoromethanesulfonyl) imide (LiTFSI) with a mass ratio of 6:4:8, a CNF/PEG gel electrolyte with high ionic conductivity was obtained (Figure 1b). In this work, we used PEG with a molecular weight of 600 Da in materials characterizations and switched to PEG dimethyl ether (PEGDME) of 500 Da in the battery tests to eliminate the detrimental effect of the active terminal hydroxyl groups of PEG on battery performances. The two PEG showed similar ionic conductivities in order of $10^{-1}$ mS cm$^{-1}$ (Figure S1, Supporting Information), which is one order of magnitude higher than that

of PEG(O) with a higher molecular weight, indicating highly similar physical properties.

By swelling the CNF membrane in salt solutions, the CNF network was stretched back into a more random orientation and the pores were opened up in the z-axis direction, as shown in **Figure 2**a,b. The salt concentration in the swelling medium dictates the balance between the concentration of immobile charges in the film and charges in the surrounding solution, thus controlling the osmotic swelling pressure.[28] This net osmotic pressure is then counterbalanced by the restraining

**ADVANCED
SCIENCE NEWS**

www.advancedsciencenews.com

**ADVANCED
FUNCTIONAL
MATERIALS**

www.afm-journal.de

**Table 1.** Properties of the CNF/PEG electrolyte membrane.

| Treatment of CNF membrane | Thickness [μm] | CNFs [wt%] | Tg [°C] | Ionic conductivity [mS/cm, R.T.] | Strength [MPa] | Break elongation [%] | Young's modulus (MPa) |
|---|---|---|---|---|---|---|---|
| 10 mM NaCl + pH2 HCl | 50 ± 3 | 21.4 | -40 | 0.023 ± 0.013 | 9.5 ± 2.2 | 23.2 ± 7.4 | 343.3 ± 107.6 |
| 5 mM NaCl + pH2 HCl | 223 ± 11 | 13.9 | -60 | 0.031 ± 0.007 | 1.5 ± 0.1 | 24.4 ± 1.1 | 21.5 ± 1.7 |
| 1 mM NaCl + pH2 HCl | 377 ± 22 | 0.9 | -65 | 0.57 ± 0.06 | 0.75 ± 0.09 | 30.7 ± 1.8 | 6.9 ± 1.0 |

network forces in the films, from the stretching of the fibrils, and this balance will determine the swelling ratio of the films. Consequently, the pore structure of the CNF network could be tuned by changing the salt concentration. The network structure created by the swelling was largely preserved after solvent exchange and the infusion of the PEG-based electrolyte,[15] without any noticeable shrinkage in apparent dimensions. At a high salt concentration of 10 mM, the resulting CNF/PEG electrolyte had a thickness of 50 ± 3 μm (Figure 2c and **Table 1**), which was slightly higher than the CNF/PEG electrolyte of which the CNFs were pretreated by acid only (30 ± 5 μm in thickness) and the dry CNF membrane (26 ± 1 μm, Figure S2, Supporting Information). In contrast, in 1 mM NaCl the CNF network significantly swelled, endowing the CNF/PEG electrolyte a thickness of 377 ± 22 μm as shown in Figure 2c. We estimated that the swelling in 1 mM NaCl solution created a porosity of ≈94% based on the thickness increase and an estimated porosity of 10–20% for the dry CNF membrane.[31] In Figure 2d,e,f, atomic force microscopic (AFM) images and the 2D wide-angle X-ray scattering (WAXS) patterns of the CNF/PEG electrolytes unveil how the concentration of the NaCl solution affected the pore structures of CNF networks. The 10 mM NaCl lead to densely packed CNFs lamella (Figure 2d) with an orientation in the x-y plane which is indicated by the poles of higher intensity in the WAXS pattern attributed to the (200) plane of CNFs. When the salt concentration was reduced to 5 mM or 1 mM, the resulting CNF/PEG electrolytes structures exhibited uniform scattering rings (Figure 2e,f) which suggest that the CNFs are de-oriented by the swelling. The 1 mM NaCl solution fully opened the pores formed by the CNF network where the fibrils were lightly entangled and highly stretched in the z-axis direction which was unveiled by the AFM image (Figure 2f). The high porosity enabled a large uptake of the active Li-ion/PEG conductive phase, while maintaining the CNFs at a minimal fraction as low as 0.9% but with a preserved continuous network structure. The AFM image also shows the CNFs were liberated from each other and reserved the few-nanometer thickness. The ultrafine network exposed a large interface area (estimated to be 670 m² g⁻¹) to accommodate the large amount of liquid-state PEG electrolyte as a homogeneous material.

The protonated carboxylic acid groups on CNF surfaces and the oxygen atoms in PEG supposedly had intimate interactions driven by the entropy increase due to the release of water and van der Waals forces.[32,33] The possible interaction between the components was investigated by using a quartz crystal microbalance with dissipation monitoring (QCM-D) and supported by a significant frequency change observed in Figure S3

(Supporting Information) when the CNFs were exposed to the PEGat pH 2, which promised a good integrity of the CNF/PEG composite. The CNF/PEG electrolyte also had a glass transition temperature ($T_g$) of −65 °C, nearly identical to that of the pristine PEG-based electrolyte (−67 °C), determined by differential scanning calorimetry (DSC) shown in Figure 2g, indicating that the PEG mobility was not significantly restricted by the CNF network. The ultra-high surface area of the CNF network allowed for a safe accommodation of the PEG electrolyte. Figure S4 (Supporting Information) shows that the samples could withstand a 33% compressive strain without any noticeable leakage of the liquid-state PEG electrolyte. The ultralow CNF content enabled an effective transformation of the liquid state electrolyte into a gel state where the mobility of the PEG-based electrolyte was to the largest extent maintained inside the porous network, thanks to the highly dispersed network made of the sparse but yet continuous, entangled CNFs. The entanglement of CNFs took place during the filtration[29] and the obtained wet filter cake was swollen into a sparse network by the 1 mM NaCl solution. For the 10 mM NaCl pre-treated film with a higher CNF fraction, $T_g$ of the CNF/PEG electrolyte increased up to −40 °C, which indicates the PEG segment mobility was hindered due to relatively higher interactions between the PEG and the CNFs at this reduced pore volume. The DSC curves (Figure 2g) and the X-ray diffraction (XRD) patterns (Figure S5, Supporting Information) both suggested that the PEG-based electrolyte show no presence of any crystalline phase. The high segment mobility of the amorphous CNF/PEG electrolyte (1 mM NaCl + pH 2 HCl treated) offered a high ionic conductivity of 0.57 ± 0.06 mS cm⁻¹ at room temperature (R.T., 22 ± 1 °C), as shown in Figure 2c. To the best of our knowledge, this is the highest R.T. ionic conductivity for a cellulose-based gel electrolyte[12,16,24–27,34] and is one of the highest values among previously reported high-performance polymer ionic conductors[11,13,35–41] (Table S1, Supporting Information).

The swelling-induced de-orientation and the reduced volume fraction of CNFs did result in a softer composite electrolyte. In water, it has been shown that the elastic modulus of these CNF networks is proportional to the volume fraction of CNFs to the power of 4,[29] and a similar relationship applies also in this case. The CNF/PEG electrolyte originating from the 10 mM NaCl + pH 2 HCl-pretreated CNF membrane exhibited a higher modulus of 343.3 ± 107.6 MPa and higher strength of 9.5 ± 2.2 MPa than the 1 mM NaCl + pH 2 HCl-pretreated sample with a modulus of 6.9 ± 1.0 MPa and strength of 0.75 ± 0.09 MPa, as shown in Figure 2h and listed in Table 1. The ionic conductivity of the latter, with an inactive materials fraction of 0.9 wt%, however, was 25 folds higher than that of the former (0.57 ± 0.06 mS cm⁻¹ versus 0.023 ± 0.013 mS cm⁻¹). The results indicated that swelling a cross-linked, in-plane

oriented CNF network in the cross-plane direction was a successful strategy to minimize the loss in mechanical integrity while improving ionic conductivity, which positioned our data points in the right-top range of the conductivity-strength map in comparison with previous reports including all types of PEG(O)-based electrolytes (Figure 2i). The results underline the ability of CNFs to form strong networks at very low volume fractions. The fact that the anisotropic swelling preserved the lateral dimension as well as the areal density of the CNFs is another factor minimizing the strength loss.

## 2.2. Enhancement of Ionic Conductivity

As shown in **Figure 3**a, the CNF/PEG electrolyte (1 mM NaCl + pH2 HCl-pretreated) showed high conductivity of 0.1 mS cm$^{-1}$ at 0 °C and 16.1 mS cm$^{-1}$ at 120 °C, promising a wide range of working temperatures for practical applications. In contrast, using a commercial polyethylene (PE) separator as the carrier, the same PEG electrolyte showed much lower ionic conductivity in the entire temperature range due to the much lower porosity (43%) of the PE separator. Particularly, at temperatures higher than 100 °C, the ionic conductivity decreased due to the poor thermal stability of PE. The comparison highlights the importance of the ultra-low CNF content in the CNF/PEG electrolyte and its excellent thermal stability. In the wide temperature range from -30 °C to 120 °C, the CNF/PEG electrolyte showed typical characteristics of ion transport in polymer gel electrolytes. Its ionic conductivity ($\sigma$) as the function of temperature ($T$) can be described by Vogel-Tammann-Fulcher (VTF) model (Equation 1):[42,43]

$$\sigma = A \exp\left(-\frac{E_a}{R\,(T - T_0)}\right) \tag{1}$$

where $A$ is the pre-exponential factor, $E_a$ the activation energy, $R$ the gas constant, and $T_0$ the Vogel temperature. The fitting (solid lines in **Figure 3**a) in the entire temperature range indicates the ions were transported by hopping under the electrical field via segment motion of PEG[4] with a very low $E_a$ of 7.1 kJ mol$^{-1}$. By comparing $A$ and $E_a$ with a variety of electrolyte systems, as shown in Figure 3b, we argue that our CNF/PEG electrolyte showed typical ion conduction characteristics of PEO/LiTFSI electrolytes while exhibiting a considerable proximity to liquid state electrolyte.[43]

Compared to the pristine PEG electrolyte, the presence of the CNF network (1 mM NaCl + pH2 HCl pretreated) increased the ionic conductivity over the entire temperature range. To understand the mechanism of such improvement, computational models were generated to simulate the ion diffusion in the CNF/PEG electrolyte system, seeking insight into the behavior of the electrolyte in the proximity of the CNF surface. Figures 3c shows the model setup with the CNF surface in the center of the simulation box and the surrounding PEGDME electrolyte. Monitoring the density profile of the pre- and post-equilibration simulation (Figure 3d; Figure S6, Supporting Information), we see that the Li$^+$, TFSI$^-$, and SCN have some affinity toward the CNF surface, possibly due to the high polarity of the abundant hydroxyl and carboxyl groups on the

surface of CNFs.[44] Table S2 (Supporting Information) illustrates the increase of Li-ion concentration from 2.054 mol L$^{-1}$ (overall Li-ion concentration) to 2.660 mol L$^{-1}$ in the first nanometer region from the CNF surface, which equivalates to ≈2% of lithium ions in this computational box. Although, when the system is equilibrated for a longer duration, the redistribution of lithium-ions toward the surface is greater, with an increase of 11.33% (Table S3, Supporting Information). This change in concentration is associated with a change in diffusion coefficient ($D_{Li}$). Focusing on the experimental concentration (2.00 mol L$^{-1}$), the ions within 1 nm from the CNF surface have the slowest $D_{Li}$, $0.47 \times 10^{-9}$ cm$^2$ s$^{-1}$, whereas in the range over 5 nm to the CNF surface, or in the "bulk" of the system, $D_{Li}$ increases to $3.00 \times 10^{-9}$ cm$^2$ s$^{-1}$, as seen in Figure 3e. The change of $D_{Li}$ at different distances also apply to simulation systems using different LiTFSI concentrations. With each concentration, the Li-ion closest to the cellulose showed reduced $D_{Li}$, which, in addition to the density profile of the simulation cell, solidifies an understanding that the CNFs are attracting Li-ion, whilst hindering their mobility. The effects of Li-ion concentration on diffusion coefficient have been illustrated previously,[45–47] which can be used to explain the difference in diffusion coefficient between the different regions of our simulation cell. If the ions are concentrated toward the CNF surface, there is a concomitant reduction in specific concentration in the bulk of the electrolyte, to which there would be an expected increase in diffusion coefficient. Nevertheless, in the simulation, this redistribution resulted in no enhancement in ionic diffusion compared to that of the pristine PEGDME electrolyte without CNFs (Table S4 and Figure S7, Supporting Information) which is distinct from the experimental findings. We argue that due to the low concentration of CNFs, the redistribution of lithium ions toward the CNF surface only affects a minimal fraction of the electrolyte in the simulation box but does not practically affect the bulk concentration (decreases by 2% only), which in turn shows little impact on $D_{Li}$ (see section Supporting Information 1. for detailed estimations).

Considering the preparation process of the CNF/PEG electrolyte, a possible explanation to the detected results could be that water has become immobilized on the cellulose surface before the inclusion of the PEG electrolyte. It is indeed often observed that removing the last strongly bound water from cellulose during drying is extremely difficult.[48,49] From the FTIR spectra in Figure S8 (Supporting Information), we found the presence of hydroxyl groups from bound water at 1641 cm$^{-1}$.[50] By performing the molecular dynamics (MD) simulations with the inclusion of strongly bound and immobile water covering the CNF surface (Figure 3f,g), we observed a significant increase in ion mobility, with the overall $D_{Li}$ increasing from $2.94 \times 10^{-9}$ to $6.68 \times 10^{-9}$ cm$^2$ s$^{-1}$ (Table S4, Supporting Information), especially for the ions closer to the surface as shown in Figure 3h. The increase in $D_{Li}$ moving away from the surface is again seen, yet with up to a fourfold increase in diffusion coefficient (Figure 3h; Table S5, Supporting Information). This analysis suggests that the immobilization of residual water on the CNF surface, prior to introducing the electrolyte, could improve the ionic mobility by disassociating more LiTFSI. This offers a hypothesis as to why the introduction of CNFs enhances ionic conductivity observed experimentally. The
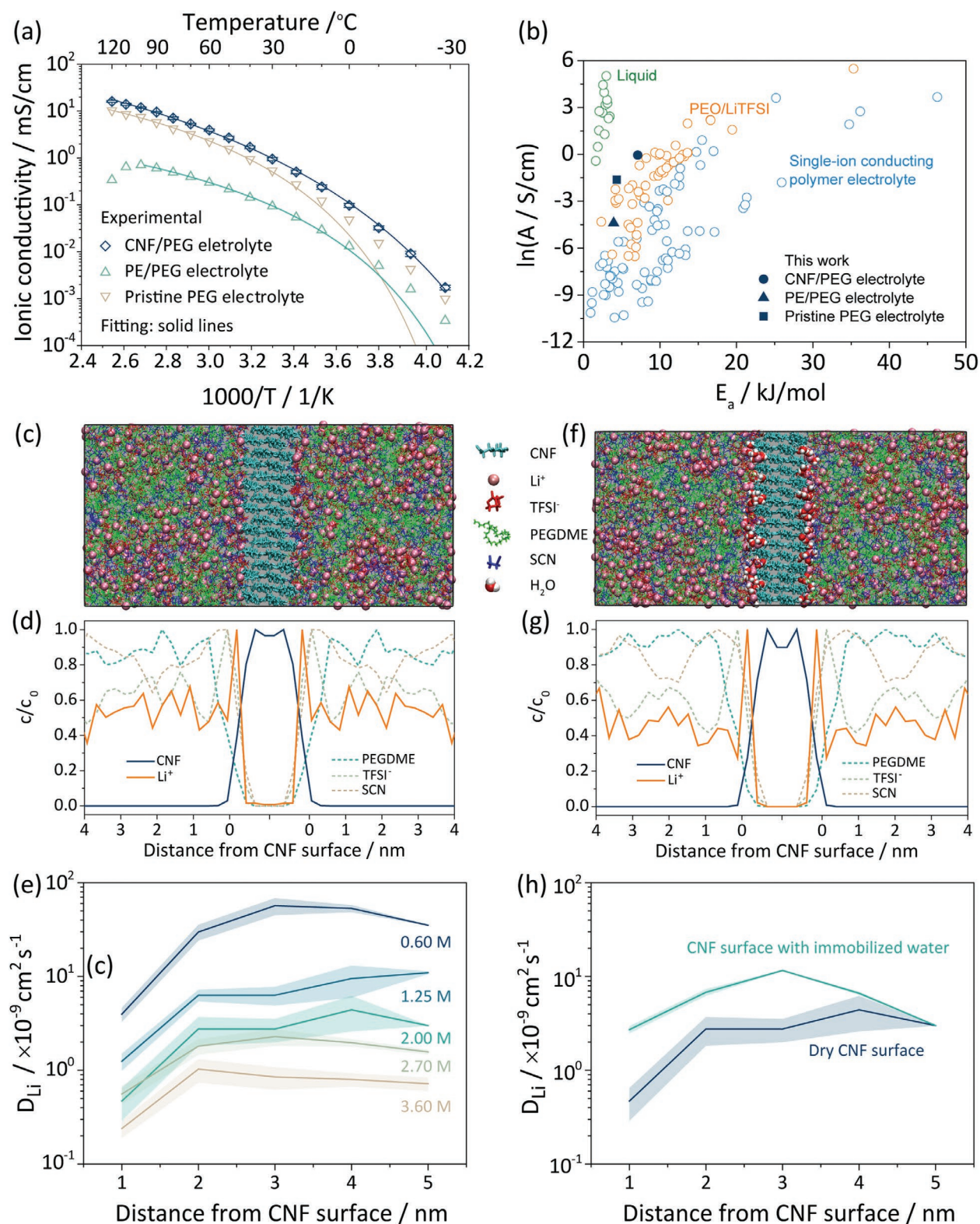
**Figure 3.** Ionic conductivity of the electrolytes. a) Ionic conductivity of the electrolytes at different temperatures; b) Natural log of the VTF prefactor as a function of the apparent activation energy for the electrolytes in comparison with different electrolyte systems;[43] c) snapshot of the simulation system consisting of CNFs and the PEGDME electrolyte; d) distribution of the PEGDME electrolyte around CNFs; e) the change of Li-ion diffusion coefficient at different distances from the CNF surface at various LiTFSI concentration; f) snapshot of the simulation system consisting a CNF, the PEGDME electrolyte, and water; g) distribution of the PEGDME electrolyte around CNFs in the presence of immobilized water; h) Li-ion diffusion coefficient of the electrolyte system with and without water.

**ADVANCED
SCIENCE NEWS**

www.advancedsciencenews.com

**ADVANCED
FUNCTIONAL
MATERIALS**

www.afm-journal.de

bound water molecules are immobilized from participating the electrochemical reactions and did not deteriorate battery performance which will be further discussed.

## 2.3. Electrochemical Performances

The high ionic conductivity and good mechanical properties of the CNF/PEG electrolyte (1 mM NaCl + pH2 HCl pretreated) promise its use as a polymer gel electrolyte. It should be noted that for PEG of low molecular weight, the terminal hydroxyl groups could deteriorate the battery performance because of the high reactivity with Li metal.[9] As shown in Figure S9 (Supporting Information), the PEG with hydroxyl groups decreased the capacity retention and coulombic efficiency (CE), leading to battery performance fading cycle by cycle. Therefore, for the battery tests, we use PEGDME of 500 Da instead of PEG of 600 Da as the two polymers have similar physical properties except for the reactivity of the terminal groups. First, we conducted a stripping/plating test at a current density of 0.1 mA cm$^{-2}$ at 60 °C, which is a typical current density for PEO-based electrolytes.[3,34,51] Owing to the high ionic conductivity (0.61 ± 0.12 mS cm$^{-1}$ at R.T., Table S4, Supporting Information), the CNF/PEGDME electrolyte showed a low and stable over potential of ≈50 mV throughout the 500 cycles of the test (**Figure 4a**), which indicates a good voltage efficiency of the cell as well as an excellent electrochemical stability. The CNF/PEGDME electrolyte maintained its functionality for at least 500 cycles without any sign of being short-circuited. The resilience to dendrite penetration is due to the densely in-plane

distributed CNFs creating a strong and ultrafine network which preserved the CNF/PEGDME electrolyte from being pierced by the potential growth of Li dendrites. We conducted cyclic voltammetry (CV) at R.T. to further investigate the electrochemical stability of the CNF/PEGDME electrolyte. As shown in Figure 4b, the CNF/PEGDME electrolyte was stable at potential up to ≈4 V versus Li/Li$^+$ where PEG started to get oxidized.[52] Minimal current response took place at ≈1 V which is normally attributed to the reactions of the anions or the impurities in polymer electrolytes.[15]

To match the potential window, lithium iron phosphate (LFP) was chosen as the cathode to assemble half-cells for performance evaluation of the CNF/PEGDME electrolyte membranes. The CV curves in **Figure 5a** obtained at 60 °C at a scan rate of 0.2 mV s$^{-1}$ showed typical redox peaks at 3.66 and 3.10 V, corresponding to the reaction of the Fe$^{2+}$/Fe$^{3+}$ couple of LFP. From the second to the fifth cycle, the CV curves were highly identical in shape, indicating a rapidly stabilized electrochemical response for the CNF/PEGDME electrolyte. Upon charging/discharging, the LFP half-cell produced a high specific capacity of 161 mAh g$^{-1}$ at 0.1C, approaching the theoretical specific capacity of LFP of 170 mAh g$^{-1}$, as shown in Figure 5b,c. The over potential of the half-cell was as low as 75 mV at 0.1C and 362 mV at 1C, owning to the high ionic conductivity of the CNF/PEGDME electrolyte. Such a high ionic conductivity also enabled the half-cell to charge/discharge at an ultrafast rate of 5C (0.88 mA cm$^{-2}$) with a specific capacity of 60 mAh g$^{-1}$. The half-cell was able to recover a high specific capacity of 159 mAh g$^{-1}$ after switching the current density back to 0.1C. As presented in Figure 5d, the CNF/PEGDME electrolyte was highly
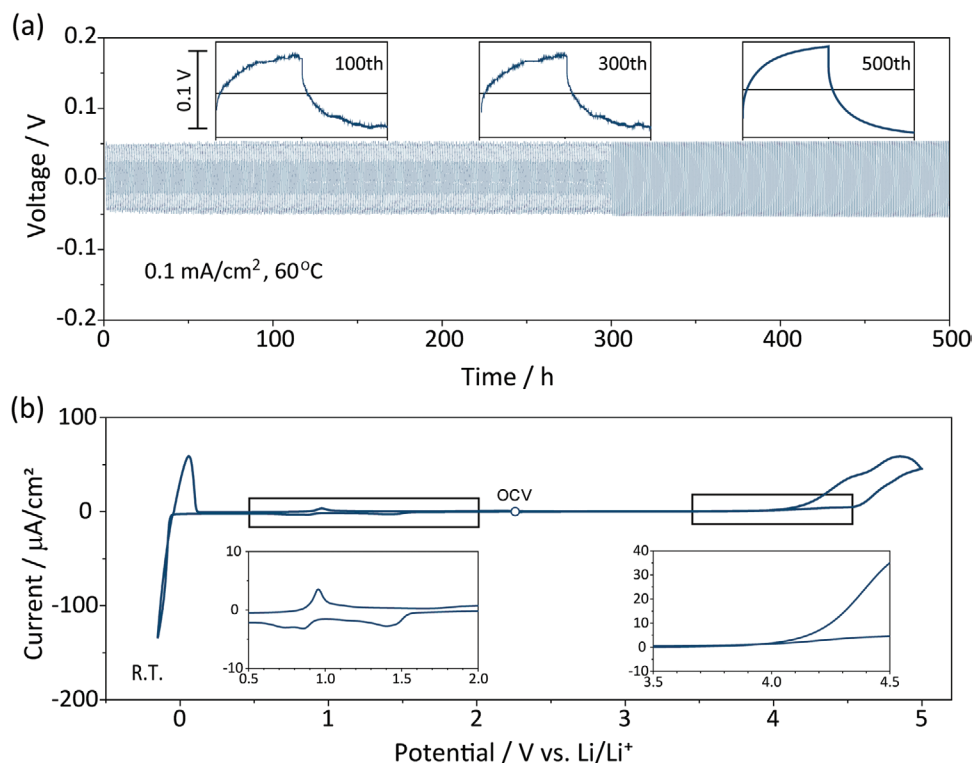


**Figure 4.** Electrochemical stability of the CNF/PEGDME electrolyte. a) Lithium stripping/plating test on the symmetric Li|CNF/PEGDME electrolyte|Li cell at 0.1 mA cm$^{-2}$; (b) CV curve of the stainless steel (SS)|CNF/PEGDME electrolyte|Li cell (insets zoom-in the range of 0.5–2.0 V and 3.5–4.5 V).
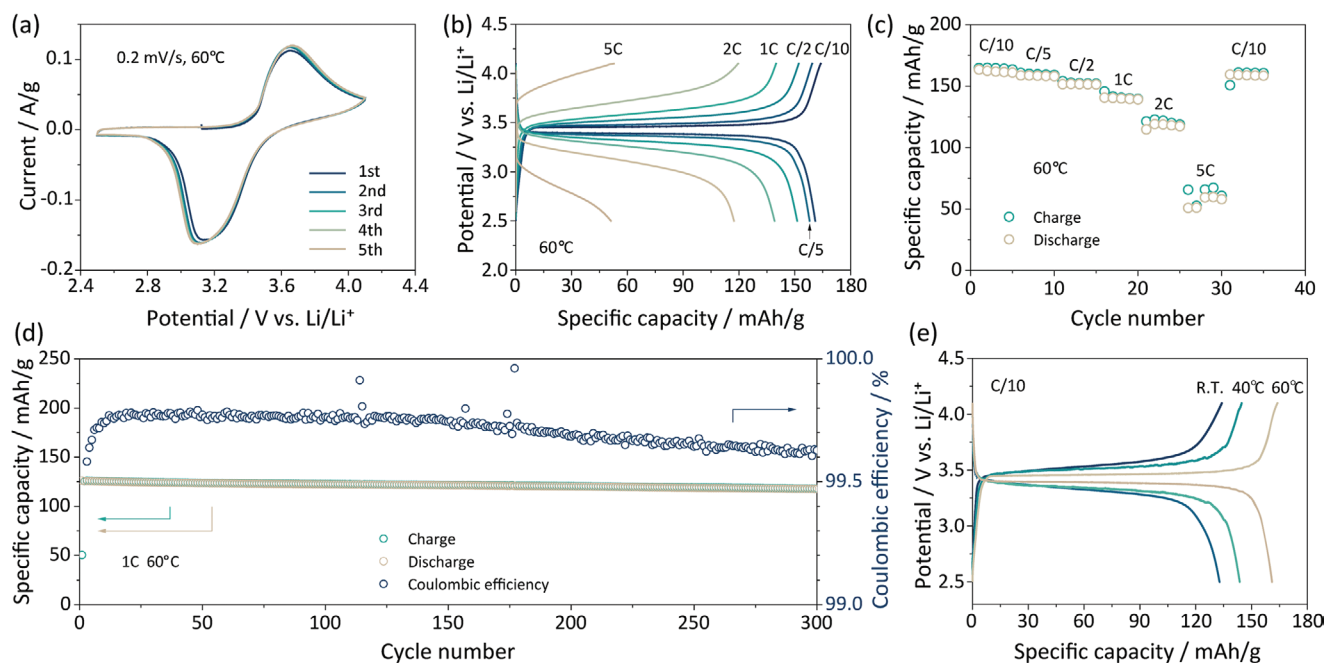
**Figure 5.** LFP|CNF/PEGDME electrolyte|Li half-cell performances. a) CV curves of the first five cycles at a scan rate of 0.2 mV s$^{-1}$, b) charge/discharge profiles at different current densities, c) rate performance, d) cycling stability, and e) charge/discharge profiles at different testing temperatures of the LFP half-cell.

stable, showing no effect from the possibly bonded water and retaining 94% of the discharge capacity of the 2nd cycle after the 300 times cycling at the high rate of 1C (corresponding to a high current density of 0.18 mA cm$^{-2}$). During the 300 cycles, the half-cell had an average CE of 99.72%, which is indicative of highly reversible battery reactions thanks to the good electrochemical stability of the CNF/PEGDME electrolyte. Figure S10 (Supporting Information) compares the electrochemical impedance spectroscopy (EIS) of the LFP half-cell before and after the cycling. The increased size of the hemi-circles in the high- to medium-frequency region indicated a higher charge-transfer resistance, suggesting the surface of cathode materials became more accessible and stabilized during the cycling. The intrinsic resistance and diffusive resistance indicated by the intercepts at the real component axis and the steep tails, respectively, did not show significant changes and suggested a stable ionic and electron conduction throughout the cycling test. An even higher current density of 0.24 mA cm$^{-2}$ was applied to stably cycle the LFP half-cell for 60 times in minimum (Figure S11a, Supporting Information). We also tested a half-cell with a high mass loading of 7.9 mg LFP cm$^{-2}$. As shown in Figure S11b (Supporting Information), at a current density of 0.1 mA cm$^{-2}$, a specific discharge capacity of 67 mAh g$^{-1}$ was obtained. This compromised performance at an even lower current density suggests that the electrode structures of the thick LFP cathode and possibly the Li foil anode as well were limiting the battery performance. Benefitting from the high R.T. ionic conductivity of the CNF/PEGDME electrolyte, the LFP half-cell delivered a high specific discharge capacity of 133 mAh g$^{-1}$ (0.1C) at R.T., as shown in Figure 5e. The half-cell also showed stable cyclic performance during the 25 cycles of charge/discharge test at R.T.,

as shown in Figure S12a (Supporting Information). The results indeed promise the practical application of the CNF/PEGDME electrolyte when working at ambient temperature. On the other hand, the increased over potential (Figure 5e) and the deteriorated rate performance (Figure S12b, Supporting Information) at lower temperature than 60 °C still limited the application to relatively low current density scenarios.

Further, we demonstrated the safety of the LFP half-cell under extreme conditions. As shown in **Figure 6**a, the good flexibility of the CNF/PEGDME electrolyte kept the pouch cell functioning after at least 5 times of fully folding and unfolding. Afterward, the same pouch cell underwent nail penetration (Figure 6b) and cut (Figure 6c), but was still able to light the LED without being short-circuited or leaking electrolyte. Further, the flame test clearly showed that the CNF/PEGDME electrolyte is safer, compared to a conventional liquid electrolyte-soaked PE separator. The CNF/PEGDME electrolyte kept its initial dimension without shrinkage and stayed retardant after being exposed to the inner flame for at least 50 s (Figure 6d). In contrast, a propylene carbonate-soaked PE separator shrank and caught fire after ignition by the inner flame for only 5s (Figure S13a, Supporting Information). Because of the organic nature, the CNF/PEGMDE electrolyte was not able to withstand the outer flame which had a higher temperature than the inner flame, and caught fire after 2s ignition (Figure S13b, Supporting Information). Nevertheless, compared to the PE separator soaked with propylene carbonate which shrank immediately and severely once in contact with the outer flame (Figure S13c, Supporting Information), there should be no doubt that the CNF/PEG electrolyte is a safer alternative to conventional liquid electrolytes.
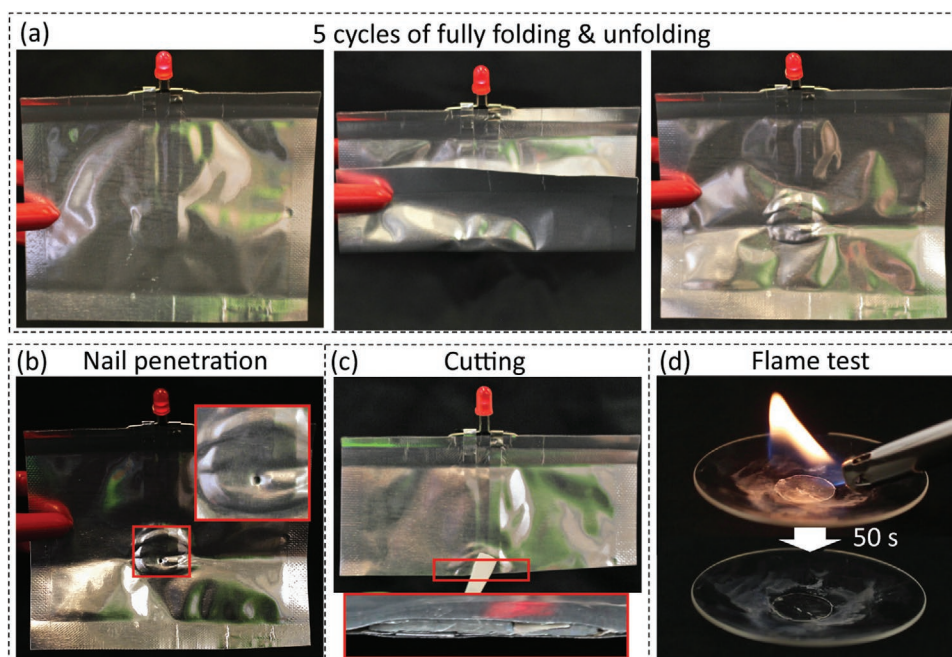
**Figure 6.** Safety demonstration. Photos showing the resilience of a pouch cell using the CNF/PEGDME electrolyte as the separator to a) folding and unfolding, b) nail-penetration, and c) cutting; d) photos showing the inner flame retardancy of the CNF/PEGDME electrolyte.

## 3. Conclusion

In conclusion, we present a novel strategy to prepare high-performance polymer gel electrolytes based on infusing liquid-state PEG electrolytes into highly porous, yet strong and flexible CNF dynamic networks. The pore openness and fibril orientation of the CNF networks, and consequently the ionic conductivity of the CNF/PEG electrolyte, were tuned by swelling the CNF network in salt solutions of different concentrations before PEG infusion. With a minimal CNF fraction of 0.9 wt%, the CNF/PEG electrolyte delivered a high R.T. ionic conductivity of $0.57 \pm 0.06$ mS cm$^{-1}$ (0.61 mS cm$^{-1}$ for the CNF/PEGDME electrolyte) and a tensile strength of $0.75 \pm 0.09$ MPa. Compared to the PEG electrolyte, the CNF dynamic network simultaneously enhanced the ionic conductivity and mechanical properties. Computational simulation indicated an affinity between Li-ion and CNFs which hinders the diffusion of Li-ion within 1 nm from CNFs. The existence of immobile water on the CNF surface, however, was found to promote the mobility of Li-ion in this interphase. We applied the CNF/PEGDME electrolyte as the separator for LFP half-cells which showed excellent performance in high specific capacity (161 mAh g$^{-1}$ at 0.1C), good rate capability (5C), cycling stability (94% capacity retention after 300 cycles at 1C) at 60 °C, as well as considerable R.T. performance and safety.

## 4. Experimental Section

*Materials*: Lithium bis(trifluoromethanesulfonyl)imide (LiTFSI, 99.95%), lithium iron phosphate (LFP, > 97%), polyethylene glycol dimethyl ether 500 Da (PEGDME), polyethylene glycol 600 Da (PEG), succinonitrile (SCN), were purchased from Sigma-Aldrich. CNFs, in a gel state with 2 wt% of nanocellulose in water, was prepared by Rise

Bioeconomy, Stockholm Sweden using a high-pressure homogenization technique. Charged carboxylic groups (448 μeq g$^{-1}$) was introduced to the CNFs by treating the sulfite-dissolving pulp of softwood with mono-chloroacetic acid.[53] The polyethylene (PE) separator was a product of SK Group (Korea) with a thickness of 20 μm and a porosity of 43%. Water used in this work was ultrapure water filtrated with a Milli-Q system.

The specific surface area (SSA) of a CNF was estimated as $\approx 670$ m$^2$ g$^{-1}$ according to Equation 2:

$$SSA = \frac{S}{m} \approx \frac{4}{t \times \rho}$$ (2)

where $S$ is the total area, $m$ the mass, $t$ the thickness of a fibril (estimated as 4 nm), and $\rho$ the density of cellulose (1.5 g cm$^{-3}$).

*Characterizations*: A Hitachi S-4800 field-emission scanning electron microscope (SEM) was used to study the micromorphology. The XRD patterns were collected with a PANalytical X'Pert PRO powder diffractometer with a Cu-K$\alpha$ source (wavelength 1.54178 Å). The 2D WAXS patterns were obtained using a single-crystal X-ray diffractometer (Bruker D8 Venture). The differential scanning calorimetry (DSC) analysis was conducted in a Mettler Toledo DSC 1 with a ramping temperature of 10°C min$^{-1}$. The mechanical property was tested in an Instron 5944 universal testing machine with a 500 N load cell. The gauge length of the specimens was 20 mm and the ramp rate was 10%/min. The samples were tested in an environment with a relative humidity of 50% after being conditioned for 24 h. A quartz crystal microbalance with dissipation (QCM-D, Model E4 from Q-Sense AB) was employed to study the interaction between CNF and PEG according to the frequency change.[54] The crystal was a QSX 303 quartz crystal sensors with a silicon oxide surface. Polyethylene amine (PEI, 600kDa-1MDa, 1 g L$^{-1}$ in water, pH 7.5) was used as the anchoring layer. The CNF dispersion was 0.1 g L$^{-1}$ at pH 6.5. The PEG solution was 1 g L$^{-1}$ at pH 2. For each layer, the adsorption time was 15 min, followed by rinsing at the corresponding pH for 15 min. The cross-sectional AFM images were collected using a MultiMode 8 AFM (Bruker, Santa Barbara, CA, USA) in the soft SCAN-ASYST (peak-force tapping) mode using TAP150 or ScanAsyst-air cantilevers. Pieces of the gel electrolytes were cut into 0.5 mm slices and attached to AFM sample discs using adhesive tape

with the cross-section facing upwards. FTIR spectra were collected on a Perkin Elmer Spectrum 100 FT-IR Spectrometer equipped with an attenuated total reflection Golden Gate (Graseby Specac) with a spectral resolution of 4 cm$^{-1}$ and 32 scans.

*Fabrication of the CNF/PEG Electrolyte*: The carboxylmethylated CNFs in water with an initial concentration of ≈2.0 g L$^{-1}$ was dispersed. Then the suspension was stirred with Ultra Turrax T25 (IKA) at 12 000 r.p.m. for 20 min, following with probe-sonication (Sonics, model CV33) of 150–200 mL suspension in an ice-bath for 10 min at 80% amplitude. After centrifuging (Mega Star 1.6R centrifuge from VWR) the suspensions at 4500 r.p.m. for 1 h, the supernatant was collected, measured for the accurate dry content of CNFs (1.94 g L$^{-1}$), and used in the following steps. The supernatant of the CNF dispersion of 40 mL was filtrated with membrane filters with 0.65 μm pore size (Millipore) where the CNFs were all collected by the filter. Typically, the wet films in a diameter of 82 mm had a solid content of 78 mg of CNFs. The CNF films were never dried and swollen in solutions of 1 mM, 5 mM, or 10 mM NaCl, followed by soaking in 0.01 M HCl solution to protonate the carboxylic groups.

The CNF films were further solvent exchanged with a mixture of ethanol and water (1:1 in volume), ethanol, ethanol and acetone (1:1 in volume), and acetone. Each step took 15 min and the samples were kept on a GFL 3015 orbital shaker. The pristine electrolyte was a mixture of PEG/SCN/LiTFSI in a weight ratio of 6:4:8. Typically, the mixture (54 g in total) was dissolved in anhydrous acetone (≈200 mL). The CNF films were soaked in the electrolyte solution until acetone evaporated all. The CNF/PEG electrolytes were vacuum-dried at 120 °C for 24 h before transferring into the glovebox. In the glovebox, the CNF/PEG electrolytes were hung to completely drain the excessive pristine electrolyte, wicked the surface with Kimwipe paper tissues, and measured the final mass of the CNF/PEG electrolytes. The fractions of CNFs in the CNF/PEG electrolytes were calculated by dividing the solid content of CNFs in the wet filter cakes with the total mass of the CNF/PEG electrolytes.

*Computational Simulation*: Cellulose Builder was used to generate the cellulose models. GROMACS was used for all MD simulations performed. The individual components of the simulation were optimized using the OPLS-AA forcefield, and input in the simulations cell using GROMACS itself. Each MD simulations was subjected to compression using the NPT ensemble (constant number of components, pressure, and temperature) for 100 ps at 1000 bar, 300 K, followed by a second equilibration at 1 bar, 300 K. Then the NVT ensemble (constant number of components, volume, and temperature) was applied at 300 K for 40 ns. For the systems involving cellulose surfaces, the cellulose surface was constrained with a force of 1000 kJ mol$^{-1}$. Temperature annealing simulations were performed using the NVT ensemble over a 5 ns time frame; increasing the temperature to 700 K over a 1 ns period, then continuation of the simulation for 2 ns at 700 K, followed by a decrease in temperature to 300 K for 1 ns and continuation until 5 ns.

Simulations including water were setup with a precursor model including only the cellulose surface and water, which was subjected to an NPT simulation to create a water monolayer. The electrolyte components were then included into space above this water layer and the simulation previous simulation steps performed for analysis. The amount of water added to the simulation was half of that of the LiTFSI; assuming a diameter of 2.75 Å for water, this was enough water to cover the surfaces of the CNF (x = 6.35 nm, y = 6.35 nm).

All data was collected using GROMACS modules, and no electrical influence was applied to the simulations. The Mean Square Displacement module was used to determine the diffusivity of components, and the diffusion coefficients were calculated using the following Equation 3:

$$\lim_{t \to \infty} \left\langle \| r_i(t) - r_i(0) \|^2 \right\rangle_{i \in A} = 6 D_A t \tag{3}$$

*Electrochemistry Tests*: All the cells were packaged inside an argon filled glovebox (MBraun Labstar) with both H$_2$O and O$_2$ levels lower than 1 ppm. The coin cells were all type CR2032. The electrochemistry tests were conducted on a Biologic VSP multichannel potentiostat equipped

with electrochemical impedance spectroscopy or a Land battery testing system (Model: CT2001A). The temperature was controlled with a fan oven. The coulombic efficiency (CE) was determined by $C_{discharge}$/$C_{charge}$*100%. The electrochemical impedance spectroscopy was carried out from 1 MHz to 10 mHz at the open circuit voltage of the cells with an amplitude of 10 mV.

The ionic conductivity ($\sigma$) was measured using a symmetric stainless steel disk (SSD)|electrolyte|SSD cell and calculated according to Equation 4:

$$\sigma = \frac{d}{R \times S} \tag{4}$$

where $d$ is the thickness of the electrolyte, $R$ the resistance of the intercept on the real axis of the Nyquist plot, and $S$ the contact area between the SSD and the electrolyte.

The Li stripping/plating test was conducted on a symmetric Li|CNF/PEG electrolyte|Li cell. The test was carried out on the Landt battery testing system for the first 300 cycles and on the Biologic potentiostat for the last 200 cycles. Each cycle lasted an hour.

The CV curve for the working window of the CNF/PEG electrolyte in Figure 4b was collected from a SS|CNF/PEG electrolyte|Li cell.

The LFP half-cells were assembled and tested in the configuration of LFP|CNF/PEG electrolyte|Li. The LFP cathodes were prepared by drop casting the slurry consisted of LFP, PEO electrolyte, and SuperP in a weight ratio of 6:3:1 on aluminum foils. The typical total mass loading was 2 mg cm$^{-2}$ for the results presented in the main text. The high loading electrode presented in Figure S11b (Supporting Information) had a mass loading of 7.9 mg LFP cm$^{-2}$. Here, the PEO electrolyte mixing with LFP and SuperP for casting the LFP cathode was PEO(400 kDa)/SCN/LiTFSI in the weight ratio of 6:4:8. 1C charge/discharge rate was defined as 170 mA/g for LFP and calculated the specific capacity of the half-cells based on the mass of the active materials.

## Supporting Information

Supporting Information is available from the Wiley Online Library or from the author.

## Acknowledgements

## Conflict of Interest

The authors declare no conflict of interest.

## Data Availability Statement

The data that support the findings of this study are available from the corresponding author upon reasonable request.

## Keywords

cellulose nanofibrils, composites, energy storages, lithium-ion batteries, polymer electrolytes

[1] N. Nitta, F. Wu, J. T. Lee, G. Yushin, *Mater. Today* **2015**, *18*, 252.

[2] M. Armand, J. M. Tarascon, *Nature* **2008**, *451*, 652.

[3] J. Wan, J. Xie, X. Kong, Z. Liu, K. Liu, F. Shi, A. Pei, H. Chen, W. Chen, J. Chen, X. Zhang, L. Zong, J. Wang, L. Q. Chen, J. Qin, Y. Cui, *Nat. Nanotechnol.* **2019**, *14*, 705.

[4] S. Xia, X. Wu, Z. Zhang, Y. Cui, W. Liu, *Chem* **2019**, *5*, 753.

[5] Z. Zou, Y. Li, Z. Lu, D. Wang, Y. Cui, B. Guo, Y. Li, X. Liang, J. Feng, H. Li, C. W. Nan, M. Armand, L. Chen, K. Xu, S. Shi, *Chem. Rev.* **2020**, *120*, 4169.

[6] S. Li, S.-Q. Zhang, L. Shen, Q. Liu, J.-B. Ma, W. Lv, Y.-B. He, Q.-H. Yang, *Adv. Sci.* **2020**, *7*, 1903088.

[7] C. Wang, W. Ping, Q. Bai, H. Cui, R. Hensleigh, R. Wang, A. H. Brozena, Z. Xu, J. Dai, Y. Pei, C. Zheng, G. Pastel, J. Gao, X. Wang, H. Wang, J.-C. Zhao, B. Yang, X. Zheng, J. Luo, Y. Mo, B. Dunn, L. Hu, *Science* **2020**, *368*, 521.

[8] Y. Jiang, X. Yan, Z. Ma, P. Mei, W. Xiao, Q. You, Y. Zhang, *Polymers* **2018**, *10*, 1237.

[9] Z. Xue, D. He, X. Xie, *J. Mater. Chem. A* **2015**, *3*, 19218.

[10] P. V. Wright, *Br. Polym. J.* **1975**, *7*, 319.

[11] J. Lopez, Y. Sun, D. G. Mackanic, M. Lee, A. M. Foudeh, M. S. Song, Y. Cui, Z. Bao, *Adv. Mater.* **2018**, *30*, 1804142.

[12] M. A. S. Azizi Samir, A. M. Mateos, F. Alloin, J.-Y. Sanchez, A. Dufresne, *Electrochim. Acta* **2004**, *49*, 4667.

[13] D. G. Mackanic, X. Yan, Q. Zhang, N. Matsuhisa, Z. Yu, Y. Jiang, T. Manika, J. Lopez, H. Yan, K. Liu, X. Chen, Y. Cui, Z. Bao, *Nat. Commun.* **2019**, *10*, 5384.

[14] W. Liu, S. W. Lee, D. Lin, F. Shi, S. Wang, A. D. Sendek, Y. Cui, *Nat. Energy* **2017**, *2*, 17035.

[15] D. Lin, P. Y. Yuen, Y. Liu, W. Liu, N. Liu, R. H. Dauskardt, Y. Cui, *Adv. Mater.* **2018**, *30*, 1802661.

[16] M. A. S. Azizi Samir, L. Chazeau, F. Alloin, J. Y. Cavaillé, A. Dufresne, J. Y. Sanchez, *Electrochim. Acta* **2005**, *50*, 3897.

[17] Z. Wang, Y. H. Lee, S. W. Kim, J. Y. Seo, S. Y. Lee, L. Nyholm, *Adv. Mater.* **2020**, *33*, 2000892.

[18] https://celluloselab.com/price/CelluloseLab%20Product%20Price%20List%202020.htm).

[19] T. Benselfelt, M. Nordenstrom, M. M. Hamedi, L. Wagberg, *Nanoscale* **2019**, *11*, 3514.

[20] H. C. Kim, J. W. Kim, L. Zhai, J. Kim, *Cellulose* **2019**, *26*, 5821.

[21] D. Klemm, F. Kramer, S. Moritz, T. Lindstrom, M. Ankerfors, D. Gray, A. Dorris, *Angew. Chem., Int. Ed.* **2011**, *50*, 5438.

[22] D. Klemm, B. Heublein, H.-P. Fink, A. Bohn, *Angew. Chem., Int. Ed.* **2005**, *44*, 3358.

[23] B. Kumar, S. J. Rodrigues, L. G. Scanlon, *J. Electrochem. Soc.* **2001**, *148*, A1191.

[24] Y. A. Samad, A. Asghar, B. S. Lalia, R. Hashaikeh, *J. Appl. Polym. Sci.* **2013**, *129*, 2998.

[25] F. Alloin, A. D'Aprea, N. E. Kissi, A. Dufresne, F. Bossard, *Electrochim. Acta* **2010**, *55*, 5186.

[26] A. Asghar, Y. Abdul Samad, B. Singh Lalia, R. Hashaikeh, *J. Membr. Sci.* **2012**, *422*, 85.

[27] M. Willgert, S. Leijonmarck, G. Lindbergh, E. Malmström, M. Johansson, *J. Mater. Chem. A* **2014**, *2*, 13556.

[28] T. Benselfelt, L. Wagberg, *Biomacromolecules* **2019**, *20*, 2406.

[29] T. Benselfelt, M. Nordenström, S. B. Lindström, L. Wågberg, *Adv. Mater. Interfaces* **2019**, *6*, 1900333.

[30] H. Kim, V. Guccini, H. Lu, G. Salazar-Alvarez, G. Lindbergh, A. Cornell, *ACS Appl. Energy Mater.* **2018**, *2*, 1241.

[31] M. Zhao, F. Ansari, M. Takeuchi, M. Shimizu, T. Saito, L. A. Berglund, A. Isogai, *Nanoscale Horiz.* **2018**, *3*, 28.

[32] T. Benselfelt, E. D. Cranston, S. Ondaral, E. Johansson, H. Brumer, M. W. Rutland, L. Wågberg, *Biomacromolecules* **2016**, *17*, 2801.

[33] M. S. Reid, M. Villalobos, E. D. Cranston, *Curr. Opin. Colloid Interface Sci.* **2017**, *29*, 76.

[34] Y. Li, Z. Sun, D. Liu, S. Lu, F. Li, G., , M. Zhu, M. Li, Y. Zhang, H. Bu, Z. Jia, S. Ding, *Energy Environ. Mater.* **2021**, *4*, 434.

[35] S. Chen, Y. Zhao, J. Yang, L. Yao, X. Xu, *Ionics* **2017**, *23*, 2603.

[36] M. Echeverri, C. Hamad, T. Kyu, *Solid State Ionics* **2014**, *254*, 92.

[37] R. He, M. Echeverri, D. Ward, Y. Zhu, T. Kyu, *J. Membr. Sci.* **2016**, *498*, 208.

[38] L. Shi, T. Zhu, G. Gao, X. Zhang, W. Wei, W. Liu, S. Ding, *Nat. Commun.* **2018**, *9*, 2630.

[39] L. Porcarelli, C. Gerbaldi, F. Bella, J. R. Nair, *Sci. Rep.* **2016**, *6*, 19892.

[40] R. Bouchet, S. Maria, R. Meziane, A. Aboulaich, L. Lienafa, J.-P. Bonnet, T. N. T. Phan, D. Bertin, D. Gigmes, D. Devaux, R. Denoyel, M. Armand, *Nat. Mater.* **2013**, *12*, 452.

[41] X. Wang, F. Chen, G. M. A. Girard, H. Zhu, D. R. MacFarlane, D. Mecerreyes, M. Armand, P. C. Howlett, M. Forsyth, *Joule* **2019**, *3*, 2687.

[42] E. Quartarone, P. Mustarelli, *Chem. Soc. Rev.* **2011**, *40*, 2525.

[43] K. M. Diederichsen, H. G. Buss, B. D. McCloskey, *Macromolecules* **2017**, *50*, 3831.

[44] L. Zhang, H. Gao, G. Jin, S. Liu, J. Wu, H. Wu, Y. Yang, Q. Wang, S. Wang, *ChemNanoMat* **2022**, *8*, 202200142.

[45] L. O. Valøen, J. N. Reimers, *J. Electrochem. Soc.* **2005**, *152*, A882.

[46] M. B. Albro, V. Rajan, R. Li, C. T. Hung, G. A. Ateshian, *Cell. Mol. Bioeng.* **2009**, *2*, 295.

[47] G. Fan, K. Pan, M. Canova, J. Marcicki, X. G. Yang, *J. Electrochem. Soc.* **2016**, *163*, A666.

[48] H. O'Neill, S. V. Pingali, L. Petridis, J. He, E. Mamontov, L. Hong, V. Urban, B. Evans, P. Langan, J. C. Smith, B. H. Davison, *Sci. Rep.* **2017**, *7*, 11840.

[49] E. L. Lindh, C. Terenzi, L. Salmén, I. Furó, *Phys. Chem. Chem. Phys.* **2017**, *19*, 4360.

[50] S. Y. Oh, D. I. Yoo, Y. Shin, G. Seo, *Carbohydr. Res.* **2005**, *340*, 417.

[51] L. Liu, J. Lyu, J. Mo, H. Yan, L. Xu, P. Peng, J. Li, B. Jiang, L. Chu, M. Li, *Nano Energy* **2020**, *69*, 104398.

[52] W. Zhou, Z. Wang, Y. Pu, Y. Li, S. Xin, X. Li, J. Chen, J. B. Goodenough, *Adv. Mater.* **2019**, *31*, 1805574.

[53] L. Wågberg, G. Decher, M. Norgren, T. Lindström, M. Ankerfors, K. Axnäs, *Langmuir* **2008**, *24*, 784.

[54] A. D. Easley, T. Ma, C. I. Eneh, J. Yun, R. M. Thakur, J. L. Lutkenhaus, *J. Polym. Sci.* **2022**, *60*, 1090.